

Scaling of fracture properties of fibre reinforced cement

C. Rieger & J.G.M. van Mier

ETH Zurich, Institute for Building Materials, Zurich, Switzerland

ABSTRACT: This paper deals with the scaling effects in uniaxial tensile tests of fibre-reinforced cement. For this purpose dogbone shaped specimens were produced in two different sizes. The small dogbone size was scaled in 3 dimensions with a factor 4. Not only the size of the specimens was scaled, the basic materials were scaled as well. A fine-grained cement and straight steel micro fibres were used for the small specimen and 4 times larger cement grains and fibres were used for the larger dogbones. The specimens were cast in a way that ensured fibre alignment in the loading direction. For the uniaxial tensile tests freely rotating supports were used and during the test the surface of the specimen was scanned with two high-resolution digital cameras. These pictures were correlated and with this displacements and strains at the surface could be calculated. Further the fiber distribution and alignment were analyzed in a cross-section close to the crack. Although the size and the material were scaled, the results show a size effect, this can be explained by the hydration products, that can not be scaled.

1 INTRODUCTION

Size and scale effects in concrete is a topic of high relevance in research. Size effect laws were derived and developed, see (Bazant 1997), (Carpinteri, Ferro, and Invernizzi 1997), (Sutherland, Sheno, and Lewis 1999), (Tucker 1927), (Danzer 2006). Weakest link theory by Weibull (Weibull 1939) was adapted to concrete and it could be shown that the relation between size and strength works for concrete structures.

$$\sigma \propto D^{-n/m} \quad (1)$$

In this relation D is the scaled size, n is the scaling dimension and m is the parameter depending on the material, see (Bazant, Xi, and Reid 1991). For normal concrete m=12 fits quite well, see (van Vliet and van Mier 2000) (for 2D scale n=2). Though it was also shown that m can vary in a wide range for concrete (Zech and Wittmann 1978).

These investigations about size effects mostly concentrate on normal concrete and on scaling the size of the specimen or structure. It is well known that for steel fibre reinforced concrete changes in fibre geometries lead to different cracking behavior of the material. Hence the effect of fibre geometry plays a big role for strength and failure behavior.

The present study concentrates both on the effect of scaling the size of the specimen as well as on the effect of scaling the basic materials used for making the specimen, see Figure 1. With this the three

dimensional scaling of the specimen size is in direct relation to the scaling of the material itself.

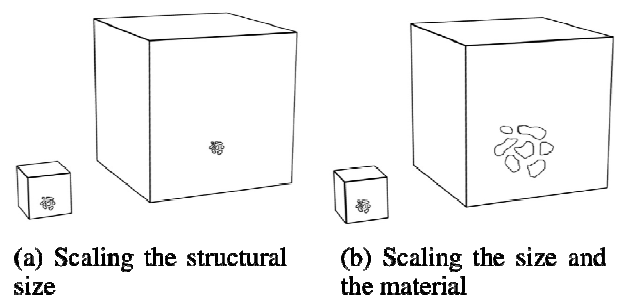


Figure 1. Schematic diagram showing scaling of structural size (a) and scaling of size and material (b).

2 MATERIALS

The uniaxial tensile tests were performed on specimens made of steel fibre reinforced cement. Tests were performed with specimens of 2 different sizes. For producing the specimens not only the size of the moulds was changed, also the basic materials were scaled. The matrix material is pure cement paste with varying water/cement-ratios. The cement is an ordinary Portland Cement (CEM I). For the small specimens a fine grained cement CEM I 52.5R with a Blaine value of 5060 cm²/g and for the large specimens a coarser cement CEM I 32.5 with a Blaine value of 2220 cm²/g was used. The grain size distribution for the different cements is listed in table 1. The grain size distribution shows that almost

all particles for the CEM I 52.5 R are smaller than 45 μm and almost all particles of the CEM I 32.5 are smaller than 200 μm . With the fine grained cement straight micro-steel fibres were used with a diameter of 50 μm and for the coarser one straight steel fibres with a diameter of 200 μm . This ensures a good packing density around the fibre, which is important for the bond between fibre and matrix.

Table 1. Grain size distribution of the different cement-types used for the specimens ($d(x\%)$ describes the particle size for which $x\%$ is smaller than d).

Grain size [μm]	CEM I 52.5 R Fraction [%]	CEM I 32.5
16	70.8	24.3
32	94.8	39.6
45	99.4	50.8
63	100	64.0
90	100	78.0
200	100	97.6
$d(10\%)$	1.6 μm	4.7 μm
$d(50\%)$	9.5 μm	44.0 μm
$d(90\%)$	26.6 μm	131.3 μm

The chemical composition is listed in table 2. The two cement-types show nearly the same chemical composition, the only big difference is the grain size distribution.

Table 2. Chemical composition of the cements used for the specimens.

Clinker Phase	CEM I 52.5 R Fraction [%]	CEM I 32.5
CaO	61.5	63.2
SiO_2	19.8	19.4
Al_2O_3	4.9	4.7
Fe_2O_3	3.3	3.2
MgO	2.1	2.2
K_2O	0.83	0.85
Na_2O	0.31	0.23

The micro-steel fibres were produced at the Institute for Building Materials. They were cut from a fine-wire. The fine-wire with a diameter of 50 μm is made of stainless steel (AISI 304L). To cut the fine-wire a special cutting machine was developed. With this machine the fibre length can be varied. For the present test series the wire was cut into fibres with a length of 3mm. For the larger specimens larger fibres were used. The fibres with a diameter of 200 μm and a length of 12 mm are industrially produced fibres and are available on the market (STRATEC). The tensile strength of the large fibres is similar to the tensile strength of the fine-wire used to produce the microfibres, see table 3.

Table 3. Tensile strength of different fibres.

Length [mm]	12	3
Diameter [mm]	0.2	0.05
Tensile strength [MPa]	2250	2400

To see the relation between fibre and matrix in the base materials, the un-hydrated cement was mixed with epoxy resin. The epoxy/cement-ratio is equal to the water/cement-ratio. The two different cements were mixed with epoxy, and in each mix the corresponding fibre was embedded. These specimens were ground and observed in the SEM. In Figures 2 and 3 the resulting grain distributions around a fibre are shown. Note, that the scale of the images differs by a factor 4 (see scale bars).

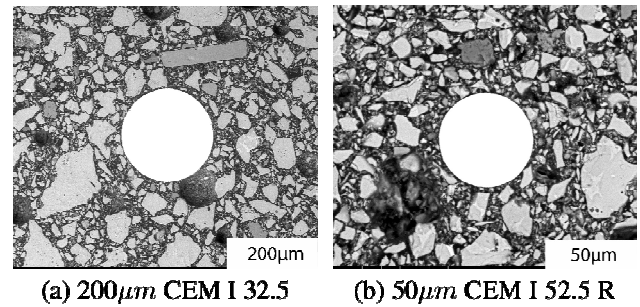


Figure 2. Relation of un-hydrated cement grains to the fibre diameter for $w/c=0.2$. The length of the whole bar in the right lower corner shows the scale of each image.

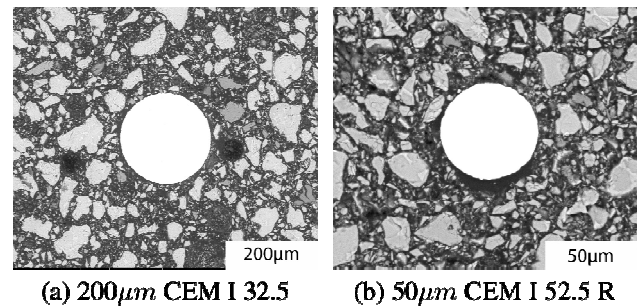


Figure 3. Relation of un-hydrated cement grains to the fibre diameter for $w/c=0.3$.

3 SAMPLE PRODUCTION

3.1 Moulds

The moulds used for casting the specimens were dogbone shaped. The small dogbones (height: 10 cm, width: 5 cm and depth: 1 cm) were scaled by factor 4 in all directions. The smallest cross-section was 10x10 mm for the small dogbones and for the larger ones 40x40 mm. The radius of the sides is half the height of the specimen (small: 5 cm, large: 20 cm), see Figure 4.

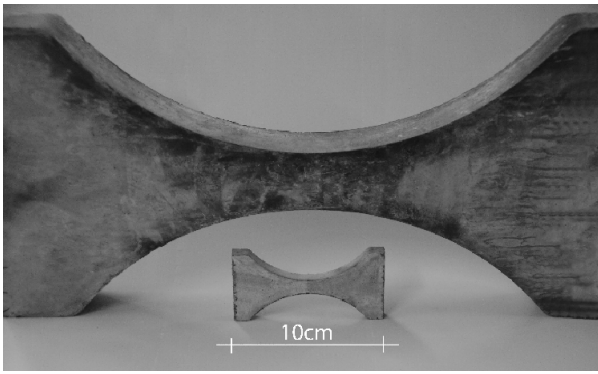


Figure 4. Picture of the two different specimen sizes.

3.2 Casting

In order to ensure a good fibre alignment, a special technique was used to cast the specimens. The fibre reinforced cement was pumped from the bottom to the top of the mould. This was done by filling the cement into a cylinder connected to the mould. By pushing the cement with a plunger into the cylinder the mould was filled from the bottom to the top, see Figure 5. Due to the flowing and climbing up in the mould, the fibres align in the narrow part of the mould. This is the part where cracks are expected to occur.

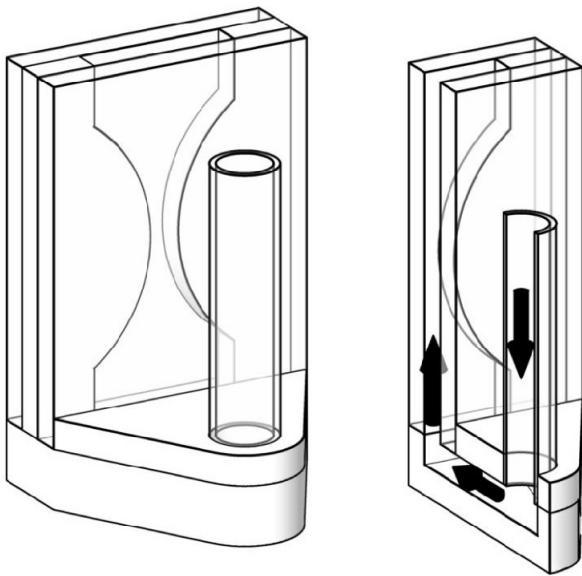


Figure 5. Schematic diagram of moulds (left) and filling method (right).

3.3 Curing

After filling the moulds were stored for 1 day in a climate chamber with 95% R.H. and 20°C. After 1 day the specimens were de-moulded and stored in tap-water for 26 days.

3.4 Preparing for Testing

At $t=21$ days of curing the specimen were cut to the required length (small: 10 cm, large: 40 cm) and put in tap water again. Next at $t=27$ days aluminum supports were glued on top and on the bottom of each specimen. To ensure parallel supports on top and on bottom the specimens were fixed in a support rig, as shown in Figure 6.

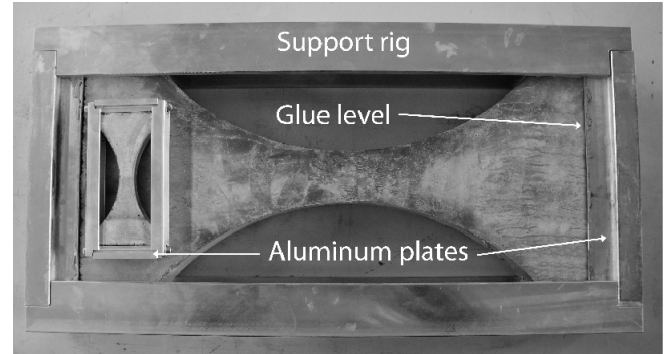


Figure 6. Fixed specimens for glueing the supports.

4 TESTING DEVICE

The uniaxial tensile tests were performed on a Zwick electro-mechanical testing machine with a capacity of 200kN. The specimens were mounted in a special rig with pendulum bars that ensures freely rotating boundary conditions in all directions (see Fig. 7).

The hinges at the rig were mounted exactly at the level where the specimen is glued to the aluminum support (see Fig. 8). Thus the rotation point is located exactly at the glue-layer between the specimen and loading plates. These experiments, as well as past experiments with identical set-ups (see for example (Stahli 2008)), show that the boundary conditions are well defined in this way.

The tests were performed under closed-loop displacement control. Two displacement transducers were mounted at the sides of the specimen. The distance between the supports before the test was $l_{0 \text{ small}} = 30\text{mm}$ and $l_{0 \text{ large}} = 120\text{mm}$. The tests were performed using the mean value of the displacements of the two sensors as control parameter. The displacement rate was $1 \mu\text{m}/\text{sec}$.

The surface of the specimens was scanned with two cameras during testing with 5 Hz. The resolution is for the small specimen at about $15 \mu\text{m}/\text{pixel}$ and for the large ones about $60 \mu\text{m}/\text{pixel}$. With digital image correlation displacements and strain concentrations can be displayed for the specimens. The setup with LVDTs and cameras is shown in Figure 9.

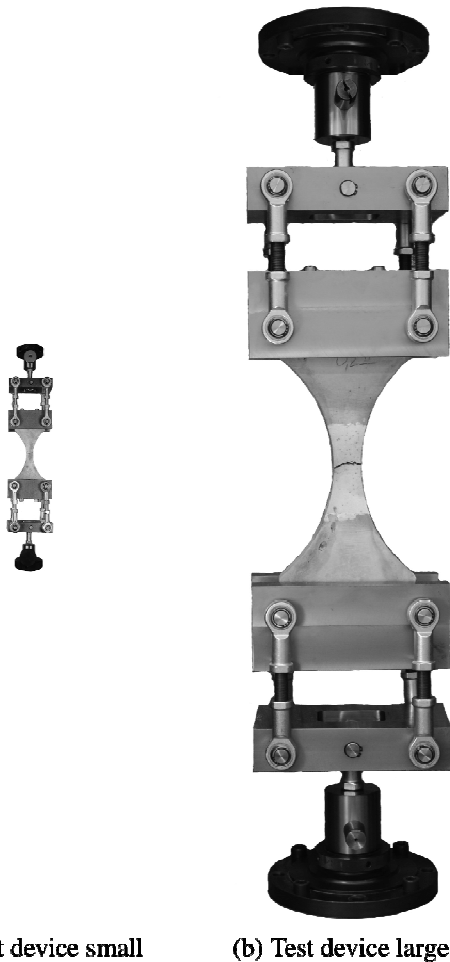


Figure 7. Testing devices for freely rotating boundaries.

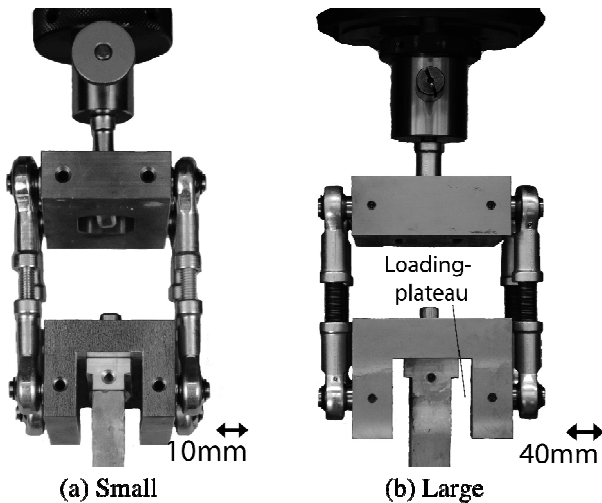


Figure 8. Side view of the two hinges.

5 RESULTS

5.1 Uniaxial Tensile Tests

As expected, higher tensile strengths were reached with lower water/cement-ratios in both specimen sizes. With $w/c=0.3$ the mean strength value reached

72% of the strength with $w/c=0.2$ in both sizes. The standard deviation of the results is higher with

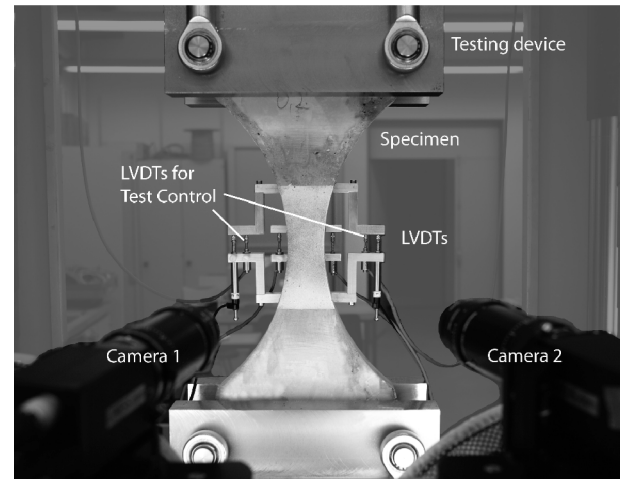


Figure 9. Test-Setup with position of LVDTs and cameras.

$w/c=0.3$ than with $w/c=0.2$, which can be explained from the higher porosity at higher w/c -ratios. The maximum stresses with the large specimens are for both w/c -ratios 73% of the small specimen, as can be seen in Figure 10.

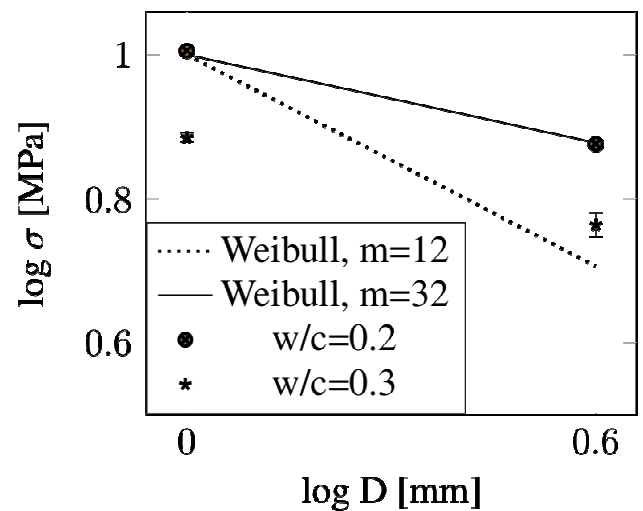


Figure 10. Maximum tensile stresses for different specimen sizes and w/c -ratios.

The stress-strain-relations for each w/c -ratio show that the post-peak behavior of the large specimens is similar to the small ones only shifted to a lower stress level (see Fig. 11 and Fig. 12). Though the pre-peak behavior is different between the two sizes. The large specimens reach the maximum stress at smaller strain values; the smaller specimens have a longer plastic plateau.

The areas under the normalized stress-strain-relations in Figures 13 and 14 were calculated until peak-load A_{npl} . These values are displayed in Figure 15. The values for A_{npl} are about 20% higher for the smaller specimens, reflecting the more non-linear pre-peak behavior.

5.2 Fibre Alignment

In order to control the fibre alignment, the specimens were cut close to the crack after testing. The cross-

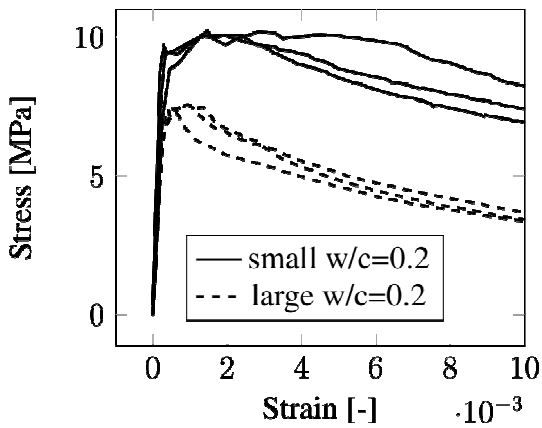


Figure 11. Stress-strain-diagrams for specimens with different sizes and $w/c=0.2$.

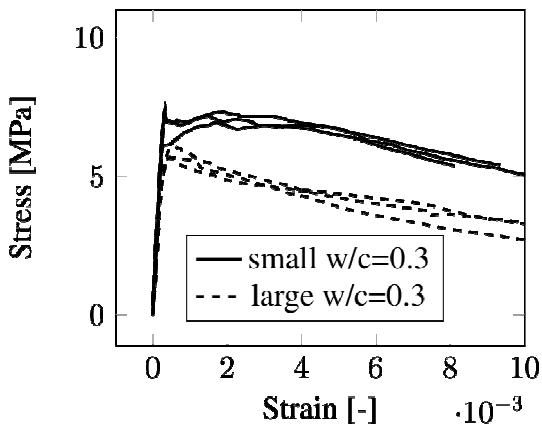


Figure 12. Stress-strain-diagrams for specimens with different sizes and $w/c=0.3$.

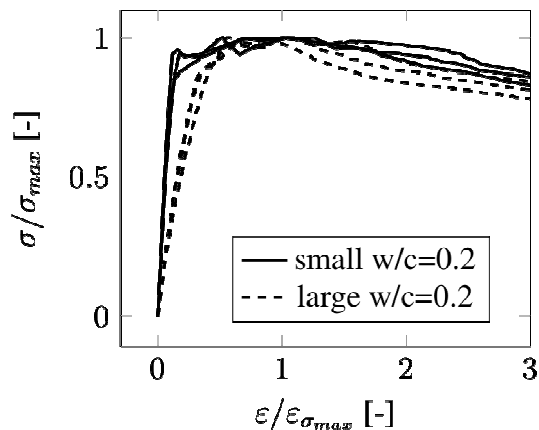


Figure 13. Normalized stress-strain-diagrams for specimens with different sizes and $w/c=0.2$.

section of the specimens was photographed and the fibre distribution over the section and the fibre alignment was checked in the picture. Next, a binary image was produced, in which only the fibres can be seen, as shown in Figure 16.

Using these pictures and an image analysis tool the center of mass of each fibre can be calculated. The amount of fibres in the section and the position of each fibre can now be determined. Additionally the outline of each fibre was drawn as an ellipse. The circularity of each ellipse was determined to see if

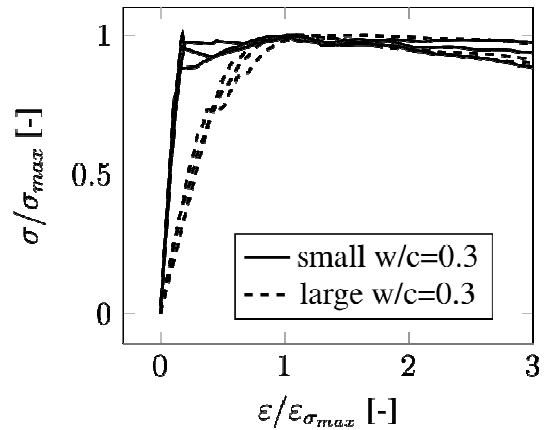


Figure 14. Normalized stress-strain-diagrams for specimens with different sizes and $w/c=0.3$.

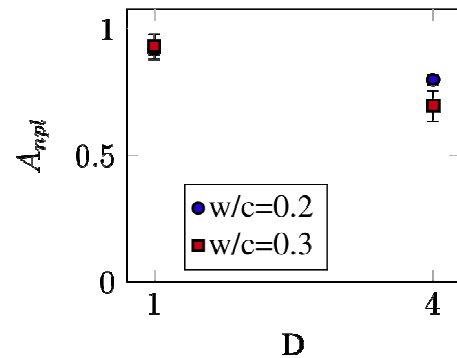


Figure 15. Area under the normalized stress-strain-relations until peak-load for different w/c -ratios.

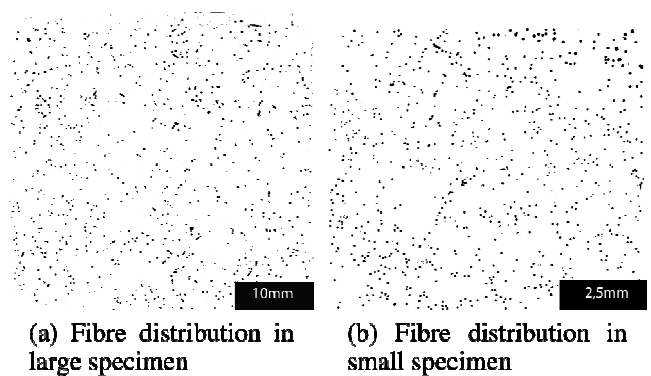


Figure 16. Binary images of cross-sections in specimens close to the crack.

the fibre is perpendicular to the cross-section (circularity=1) or intersects at an angle (circularity<1), see Figures 17 and 18.

The histograms show that in most of the specimens the fibres are aligned very well. The circularity is very close to 1. The only exception is the small se-

ries with $w/c=0.3$, which shows a larger amount of unaligned fibres than the other series.

With the binary images it was possible to count the fibres in the cross-section. Figure 19 shows the average amount of fibres and the minimum and maximum values for each testing series.

The cross-sections of the small specimens show a

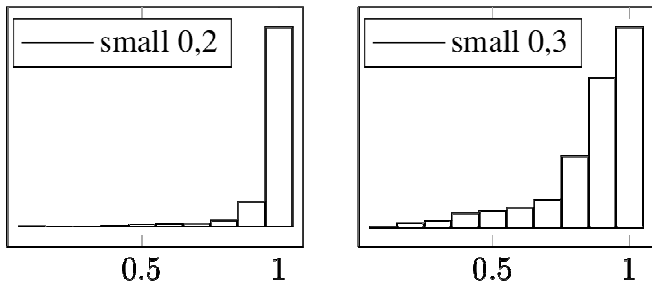


Figure 17. Histogram of circularity for all small specimens with $w/c=0.2$ (left) and $w/c=0.3$ (right).

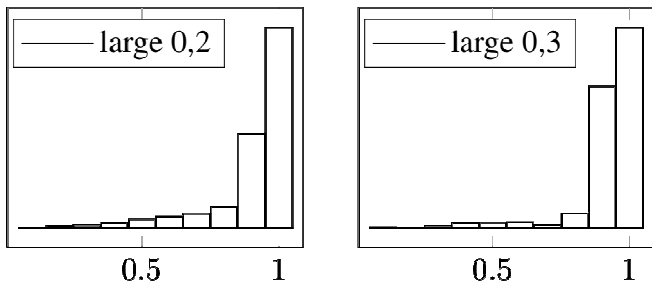


Figure 18. Histogram of circularity for all large specimens with $w/c=0.2$ (left) and $w/c=0.3$ (right).

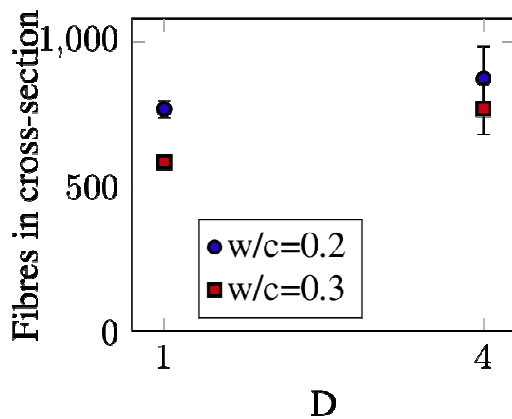


Figure 19. Fibre amount in cross-section for different specimen sizes and w/c -ratios.

slightly smaller amount of fibres than the large specimens. With $w/c=0.3$ less fibres were counted than with $w/c=0.2$ for both types of specimens. The large specimens show a higher variation in the fibre amount than the small specimens.

5.3 ESEM Investigations

The same specimens like shown in Figures 2 and 3 were produced with the real material used for the tested specimens. That means small fibres were embedded in fine grained cement with w/c -ratios 0.2 and 0.3 and the same was done with large fibres in the coarse grained cement. The specimens were cured in the same way the large specimen were cured and after 28 days they were embedded in epoxy resin. The specimens were ground and polished and the cross-sections were observed in ESEM (Figs. 20 and 21).

The pictures of the cross-sections look similar for equal w/c -ratios. The area of the unhydrated cement-

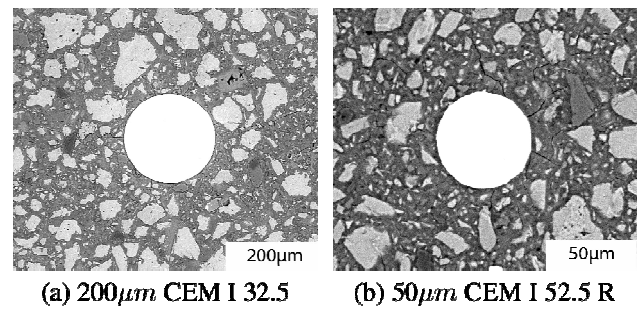


Figure 20. Relation of hydrated cement grains to the fibre diameter for $w/c=0.2$.

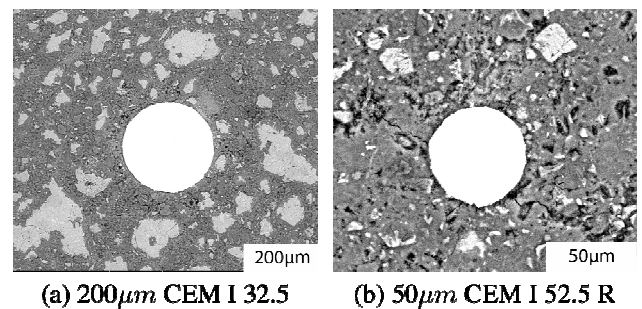


Figure 21. Relation of hydrated cement grains to the fibre diameter for $w/c=0.3$.

particles in the cross-section was determined with image analysis. For this the average fraction of unhydrated cement particles around the fibres in the cross-section was determined, as well as the fraction of particles in circles around the fibre to see the influence of distance from fibre to the amount of unhydrated cement particles. The results of this analysis are shown in table 4 for the cross-sections after 28 days (Figs. 20 and 21) as well as for the unhydrated particles embedded in epoxy resin (Figs. 2 and 3). For equal w/c -ratios the areas of unhydrated cement-particles to the area of the entire cross-section A_{uh}/A_{cs} is similar. This shows that the material scaling worked on that level.

Table 4. Average area of unhydrated cement particles in a cross-section.

Fibre diameter	w/c=0.2	w/c=0.3
50 μm in CEM I 52,5 R un-hydrated in epoxy	36.6%	31.4%
50 μm in CEM I 52,5 R after 28 days	24.5%	7.7%
200 μm in CEM I 32,5 un-hydrated in epoxy	38.6%	32.6%
200 μm in CEM I 32,5 after 28 days	27.0%	11.4%

One can see a big difference between the particles in epoxy and after 28 days. The difference between w/c-ratio 0.2 and 0.3 is much larger after 28 days.

Figures 22 and 23 show a clear tendency. Close to the fibre less un-hydrated cement particles can be found for the epoxy cross-section as well as for the 28 days old cross-section and for both sizes.

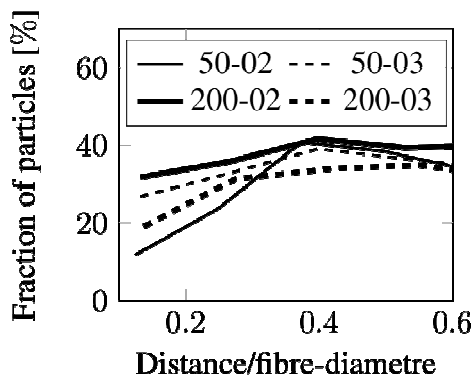


Figure 22. Fraction of unhydrated cement particles around a fibre in epoxy resin.

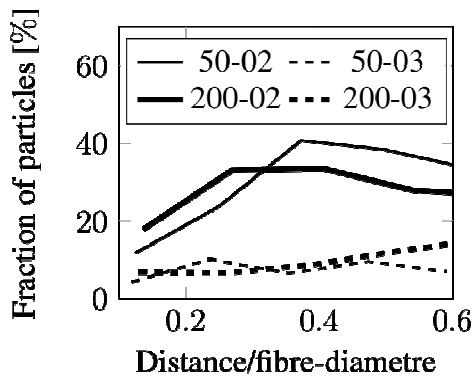


Figure 23. Fraction of unhydrated cement particles around a fibre after 28 days.

6 DISCUSSION

Although the specimen size as well as the material were scaled, the results of the uniaxial tensile tests show a size effect. The maximum tensile strength decreases with increasing size, as is known from many experiments.

The pre-peak-behavior of the two different sizes also show differences. The smaller specimens show a much more distinctive pre-peak-behavior than the large ones. The strain capacity at peak load is higher with smaller size than with the large sized specimens. For an explanation of these results one has to question if the whole material structure is scaled. For this study the basic materials like fibres and cement grains were scaled and the investigations show that the fibre alignment, as well as the fibre distribution over the specimen cross-section is similar for both sizes. Also the amount of un-hydrated cement particles around the fibre seems to be equivalent for small and large specimens. The distribution of the particles around the fibre shows that for both the small and the scaled material less particles can be found close to the fibre. A reason for this distribution can be a wall effect similar like observed in the interface between matrix and aggregates in normal concrete, see (Scrivener 2004). At the microscale the materials seem to be scaled quite accurately and one could discuss about external influences like shrinkage, moisture- or temperature gradients, that can have an influence on the strength of the material. This could be a possible approach to explain the decreasing strength. It is well known that the fibre bond is an important factor for strength and fibre pullout resistance. The fibre bond at the microlevel seems to be similar for both sizes, but by looking with a higher magnification at a fracture surface of the material one can see the hydration products like CSH needles and calcium-hydroxyde. Calcium-hydroxyde ($\text{Ca}(\text{OH})_2$ or CH in cement-notation) can easily be recognized because it has a typical shape (hexagonal plates). These plates were found in both materials in the same size, see Figure 24.

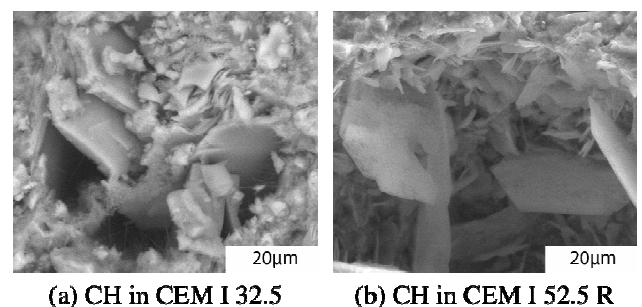


Figure 24. Calcium-hydroxyde plates in small and large scaled material.

These results indicate that although the basis materials were scaled, the hydration products can not be scaled. These hydration products are responsible for the bond between fibre and matrix. It is obvious that different fibre sizes in the same surrounding matrix lead to a different fibre pullout behavior. This could be a possible explanation for the different pre-peak-behavior.

In order to confirm this statement further investigations of the interface between fibre and matrix have to be done. The analysis of the pictures taken during the tests can also help to find explanations for the different behavior. With digital image correlation displacement vectors and strains can be calculated and visualized. With such results at hand the crack initiation and crack growth can be analyzed in great detail. At the moment these analyses have not been fully completed and will be published in a forthcoming paper.

7 CONCLUSIONS

In this paper the size effect when not only the specimen size is scaled but also the material itself is studied. Dogbone shaped specimens were produced and scaled in three dimensions with a factor 4. These two sizes were tested. The basic materials the specimens were made of were also scaled. The fibres as well as the cement grains were scaled by the same factor 4. ESEM investigations of polished cross-sections of the different materials show that the scaling on micro-level worked quite well. The unhydrated as well as the hydrated cement particles show for each w/c-ratio with different sizes the same area fraction. With image analysis the distribution of unhydrated cement particles was determined. With the small as well as with the large fibre less particles close to the fibre can be found.

The specimens were produced with a technique that ensures fibre alignment. With image analysis the pictures of cross-sections close to the crack the circularity and the fibre amount in the cross-section was determined. The results show that the fibres were mostly aligned in the loading direction.

The uniaxial tensile tests show lower strengths for the larger sized specimens. The decreasing strength with increasing size can be described for w/c=0.2 with a Weibull-modulus of $m = 32$. The results also show a much more distinctive pre-peak-behavior for the smaller sized specimens. A possible explanation for this can give the hydration products that are responsible for the fibre-matrix bond. ESEM investigations of fractured surfaced show that the hydration products could not be scaled. This can be a possible reason for the different pre-peak behavior. During the tests the specimens were scanned with high-resolution digital cameras. With digital image correlation displacements and strains will be calculated, which may give further explanations for the differences observed in the tests.

ACKNOWLEDGMENTS

The support of Mr. Erich Ritschard of Holcim AG, who provided the cement, the support of the mechanical workshop, Mr. Peter Jenny and Mr. Mariano Pauli, the support of Mr. Heinz Richner and the support with ESEM measurements and ESEM pictures by Mrs. Gabriele Peschke is kindly acknowledged.

REFERENCES

- Bazant, Z. P. (1997). Scaling of quasibrittle fracture: Hypotheses of invasive and lacunar fractality, their critique and weibull connection. *International Journal of Fracture* 83(1), 41–65.
- Bazant, Z. P., Y. P. Xi, and S. G. Reid (1991). Statistical size effect in quasi-brittle structures 1: Is weibull theory applicable. *Journal of Engineering Mechanics-ASCE* 117(11), 2609–2622.
- Carpinteri, A., G. Ferro, and S. Invernizzi (1997). The nominal tensile strength of disordered materials: A statistical fracture mechanics approach. *Engineering Fracture Mechanics* 58(5-6), 421 – 435.
- Danzer, R. (2006). Some notes on the correlation between fracture and defect statistics: Are weibull statistics valid for very small specimens? *Journal of the European Ceramic Society* 26(15), 3043 – 3049.
- Scrivener, K. L. (2004). Backscattered electron imaging of cementitious microstructures: understanding and quantification. *Cement and Concrete Composites* 26(8), 935 – 945.
- Scanning electron microscopy of cements and concretes.
- Stahli, P. (2008). Ultra-Fluid, Oriented Hybrid-Fibre-Concrete. Dissertation, ETH Zurich.
- Sutherland, L. S., R. A. Sheno, and S. M. Lewis (1999). Size and scale effects in composites: I. literature review. *Composites Science and Technology* 59(2), 209 – 220.
- Tucker, J. (1927). A study of the compressive strength dispersion of materials with applications. *Journal of the Franklin Institute* 204(6), 751 – 781.
- van Vliet, M. R. A. and J. G. M. van Mier (2000). Experimental investigation of size effect in concrete and sandstone under uniaxial tension. *Engineering Fracture Mechanics* 65(2-3), 165 – 188.
- Weibull, W. (1939). A statistical theory of the strength of materials. *Proceedings of the Royal Swedish Institute for Engineering Research* 151.
- Zech, B. and F. Wittmann (1978). Part ii probabilistic approach to describe the behaviour of materials. *Nuclear Engineering and Design* 48(2-3), 575 – 584.